DDX54 downregulation enhances anti-PD1 therapy in immune-desert lung tumors with high tumor mutational burden

Jeong-Ryeol Gong[a,1], Jungeun Lee[a,1] (ID), Younghyun Han[a], and Kwang-Hyun Cho[a,2] (ID)

Affiliations are included on p. 12.

High tumor mutational burden (TMB-H) is a predictive biomarker for the responsiveness of cancer to immune checkpoint inhibitor (ICI) therapy that indicates whether immune cells can sufficiently recognize cancer cells as nonself. However, about 30% of all cancers from The Cancer Genome Atlas (TCGA) are classified as immune-desert tumors lacking T cell infiltration despite TMB-H. Since the underlying mechanism of these immune-desert tumors has yet to be unraveled, there is a pressing need to transform such immune-desert tumors into immune-inflamed tumors and thereby enhance their responsiveness to anti-PD1 therapy. Here, we present a systems framework for identifying immuno-oncotargets, based on analysis of gene regulatory networks, and validating the effect of these targets in transforming immune-desert into immune-inflamed tumors. In particular, we identify DEAD-box helicases 54 (DDX54) as a master regulator of immune escape in immune-desert lung cancer with TMB-H and show that knockdown of DDX54 can increase immune cell infiltration and lead to improved sensitivity to anti-PD1 therapy.

DDX54 | immuno-oncotargets | tumor mutational burden | anti-PD1 therapy | systems biology

Immune checkpoint inhibitor (ICI) therapy has dramatically improved survival rates and induced sustainable long-term responses in many patients with various cancers that were previously untreatable (1, 2). Nevertheless, the efficacy of ICI therapy remains restricted to a minor subset of patients (3, 4). Furthermore, despite endeavors to augment its response rate through combination therapies, the success rate remains inadequate (5). To address this problem, we sought to directly address the cause of the immune evasion mechanisms of cancer cells, rather than to induce only the activation of immune cells.

Previous studies on the anticancer mechanisms of ICI therapy suggested that such ICI therapy could reinvigorate preexisting T cells in cancer tissue and that those T cells could induce cancer cell death. However, it was revealed that the T cells that infiltrated into cancer tissues had already been exhausted and could not be reinvigorated by ICI therapy due to epigenetic scarring of T cells (6). In addition, single-cell T cell receptor analysis revealed that in patients responsive to ICI therapy, expansion of newly infiltrated T cell clones is induced following ICI therapy, rather than expansion of preexisting T cell clones within the cancer tissues (7). Together, these suggest that to improve the efficacy of ICI therapy, we need to block the mechanisms that inhibit T cell infiltration into cancer tissues and induce the expansion of infiltrated novel T cell clones.

Immune cells recognize cancer mutations as non-self-antigens, so accumulations of immune cells can facilitate infiltration of T cells and thereby enhance the efficacy of ICI therapy. From this, a high tumor mutation burden (TMB-H) has been approved by the US Food and Drug Administration (FDA) as a favorable predictive biomarker for ICI therapy efficacy across various cancers (8, 9). However, despite the role of tumor mutation as a recognizable marker of cancer to ICI therapy, its effectiveness in identifying patients who might respond to ICI therapy is still limited. This limitation might arise from the fact that the antigen-processing procedure of cancer mutations for immune cell recognition and the subsequent clearance of recognized antigens are both long and complicated processes. Such mechanisms aim to prevent any possible self-damage that might be caused by the activation of aberrant immune cells. Interestingly, cancer cells still exploit such mechanisms to evade immune surveillance by interrupting those procedures at various points (10).

To enhance the efficacy of ICI therapy, it is important to induce the infiltration of new T cells into the cancer cells. However, cancer cells inhibit immune cell infiltration by activating several oncogenic pathways such as Wnt3a–β-catenin and Myc pathways (10). Identifying a master regulator that plays a central role in these pathways by inhibiting the

Significance

Although a high mutational burden is an FDA-approved biomarker for immune checkpoint inhibitors (ICIs), some immune-desert lung cancers remain resistant despite a high tumor mutational burden (TMB-H). We identified DDX54 as a master regulator in immune-desert lung cancer with a high mutational burden, whose knockdown reduces resistance to ICIs. DDX54 promotes an immune-evasive tumor microenvironment (TME) in lung cancer by inducing CD38 and CD47 expression and inhibiting immune cell infiltration, thereby reducing the efficacy of ICIs. DDX54 knockdown combined with anti-PD-1 treatment increases T cell, NK cell, and antitumor monocyte infiltration, sensitizing tumors to anti-PD-1 therapy. These findings suggest that targeting DDX54 can reprogram immune-desert tumors into immune-inflamed tumors, potentially enhancing immunotherapy efficacy in cancer patients.

[1]J.-R.G. and J.L. contributed equally to this work.

[2]To whom correspondence may be addressed. Email: ckh@kaist.ac.kr.

infiltration of T cells into cancer cells is crucial for the development of a combination therapy enhancing the efficacy of ICI therapy. In this study, we particularly focused on lung cancer samples that, even with their TMB-H, exhibited a high proportion of patients with reduced T cell infiltration. We collected lung cancer data from The Cancer Genome Atlas (TCGA) that meet the FDA approval criteria (10 mutations/Mb) without mutations in the antigen presentation pathway. Using these samples, we inferred a gene regulatory network and found a master regulator, DEAD-Box Helicase 54 (DDX54) that mediates immune escape features in the groups with both sufficient mutation and low immune cell infiltration. This led us to identify an immuno-oncotarget, DDX54, which appears to be critical in hindering immune cell infiltration into tumor tissues and contributes to resistance against ICI therapy.

It is known that controlling regulators, which are important in T cell infiltration into cancer tissue, may also enhance the therapeutic effect of ICI therapy. Indeed, by both knockdown of DDX54 and anti-PD1 treatment, we could effectively induce the infiltration of immune cells into cancer tissue and thereby inhibit the proliferation of ICI therapy-resistant lung cancer cells. We further found that the knockdown of DDX54 suppresses the activity of oncogenic pathways such as Jak-Stat3, Wnt3a–β-catenin, and Myc, and also induces the expression of tumor-suppressive microRNAs such as miR-34b-5p (11). Our study provides insights into enhancing the effects of ICI therapy by inhibiting the mechanism by which cancer cells evade immune cell infiltration, rather than solely inducing the activity of immune cells that directly kill cancer cells.

Results

In Lung Adenocarcinoma (LUAD), a Significant Proportion of Samples Exhibit Suppressed Lymphocyte Infiltration Despite TMB-H.
To investigate whether lymphocyte infiltration is suppressed despite cancer cells being recognized as nonself by immune cells, we collected data on lymphocyte infiltration patterns and degrees of mutations from TCGA. Then, we excluded samples containing mutations in the antigen processing and presentation pathway, since such samples typically fail to present antigens regardless of their mutation levels and are not typically recognized as nonself by immune systems. Among the selected samples, those with a mutation burden greater than 10 mutations/Mb were designated TMB-H and those with less than 10 were designated low tumor mutation burden (TMB-L). This threshold is approved by the FDA as a biomarker for ICI therapy (8). Hence, we defined TMB-H as samples that could be recognized as nonself by the immune system. To further classify these samples based on immune infiltration, we utilized preclassified human tumor data from Saltz et al. (12), which categorized tumors into three types—inflamed, excluded, and desert—based on histological analysis. Since our study focuses on immunotherapy resistance driven by intrinsic cancer cell characteristics, we excluded immune-excluded tumors, as they primarily evade immune surveillance through stromal cell effects. We categorized the samples as immune-desert when no immune cell infiltration is observed in the cancer tissue (13), and as immune-inflamed when there is evident lymphocyte infiltration (Fig. 1A). Intriguingly, as shown in previous studies (14, 15), approximately 30% of the selected pan-cancer samples with both TMB-H and intact antigen processing and presentation pathways exhibit an immune-desert phenotype. Notably, within the TMB-H samples, the mutation burden did not significantly differ between samples with high and low immune cell infiltration (Fig. 1B). Next, we further investigated how the proportion of samples with "TMB-H and immune-desert" varies across different

organs. We found a range of such proportions in various tumors, with LUAD being particularly notable (Fig. 1C). In LUAD, the proportion of these cells is significantly elevated, and it also has the highest number of such samples. Therefore, we aimed to discern the attributes of LUAD samples with TMB-H that exhibit an immune-desert profile by comparing those with high versus low immune cell infiltration. By gene set enrichment analysis (GSEA), we found that immune-desert samples with TMB-H are associated with multiple immune suppressive pathways and signatures such as WNT3A and MYC pathway, epithelial–mesenchymal transition (EMT), and cancer-associate stemness (*SI Appendix*, Fig. S2). On the other hand, we found that immune-inflamed samples with TMB-H are associated with activation signatures of immune cells including T cells and NK cells (*SI Appendix*, Fig. S2) in various cancer types. From these results, we were intrigued whether we can revert immune-desert with TMB-H to immune-inflamed with TMB-H by regulating the primary features of immune-desert with TMB-H, and thereby upregulate the responsiveness of ICI therapy.

DDX54 Is Identified as a Master Regulator that Orchestrates Suppressed Lymphocyte Infiltration Even with TMB-H in Lung Cancer.
We found that immune cell infiltration could be inhibited in some cancer tissues that have TMB-H with a normal antigen presentation pathway. In these samples, we also found that the functions of various immune cells are suppressed (*SI Appendix*, Fig. S2). Therefore, we aimed to identify the master regulators within cancer cells that control these features. As defined in previous studies (16, 17), master regulators are a small number of genes that govern the state of a cell by controlling gene expression and determining the activity of pivotal transcriptome factors (TFs). From this definition, we aimed to identify the master regulator that can control these immune-desert features at the top of the gene regulation in cancer cells. For this purpose, we performed an interactome analysis to infer the relationship between TFs and their target genes using LUAD transcriptome data of TCGA and to construct a gene regulatory network (GRN). By integrating the GRN with the LUAD transcriptome data, we inferred the pivotal TFs of cells that have both TMB-H and suppressed immune cell infiltration (18–20) (Fig. 2A, for further details, refer to the *Detailed Methods* in *SI Appendix* details). Interestingly, NR3C1 (encoding glucocorticoid receptor) (21) and CHAF1A (22) of the inferred pivotal TFs were identified from previous experimental studies to play important roles in ICI treatment. All of these pivotal TFs significantly increased the expression of TF-regulated genes (TF activity) in samples with inhibited T cell infiltration, but the expression of the TFs did not increase according to T cell infiltration (Fig. 2B and *SI Appendix*, Fig. S3). Therefore, we speculated that the genes regulated by these TFs might not be regulated depending on the expression of the TFs, but instead might be coregulated together by factors (master regulators) that determine the activity of these pivotal TFs. To identify the master regulator of the selected pivotal TFs, we computed the regulator score based on the conditional mutual information among the master regulators, target genes, and pivotal TFs (Fig. 2 C and D, for further details, refer to the *Detailed Methods* in *SI Appendix*). As a result, we found DDX54, which showed the highest regulator score and the most significant increase in gene expression, as the master regulator of cancer cells with suppressed immune cell infiltration. Of note, four other master regulator candidates ranked below DDX54 such as ATP2A2, RACGAP1, PTPN11, and PCNA were previously studied and suggested to potentially increase the effectiveness of immunotherapy (23–26) (Fig. 2 C and D, see the full list of master regulators that govern immune-desert
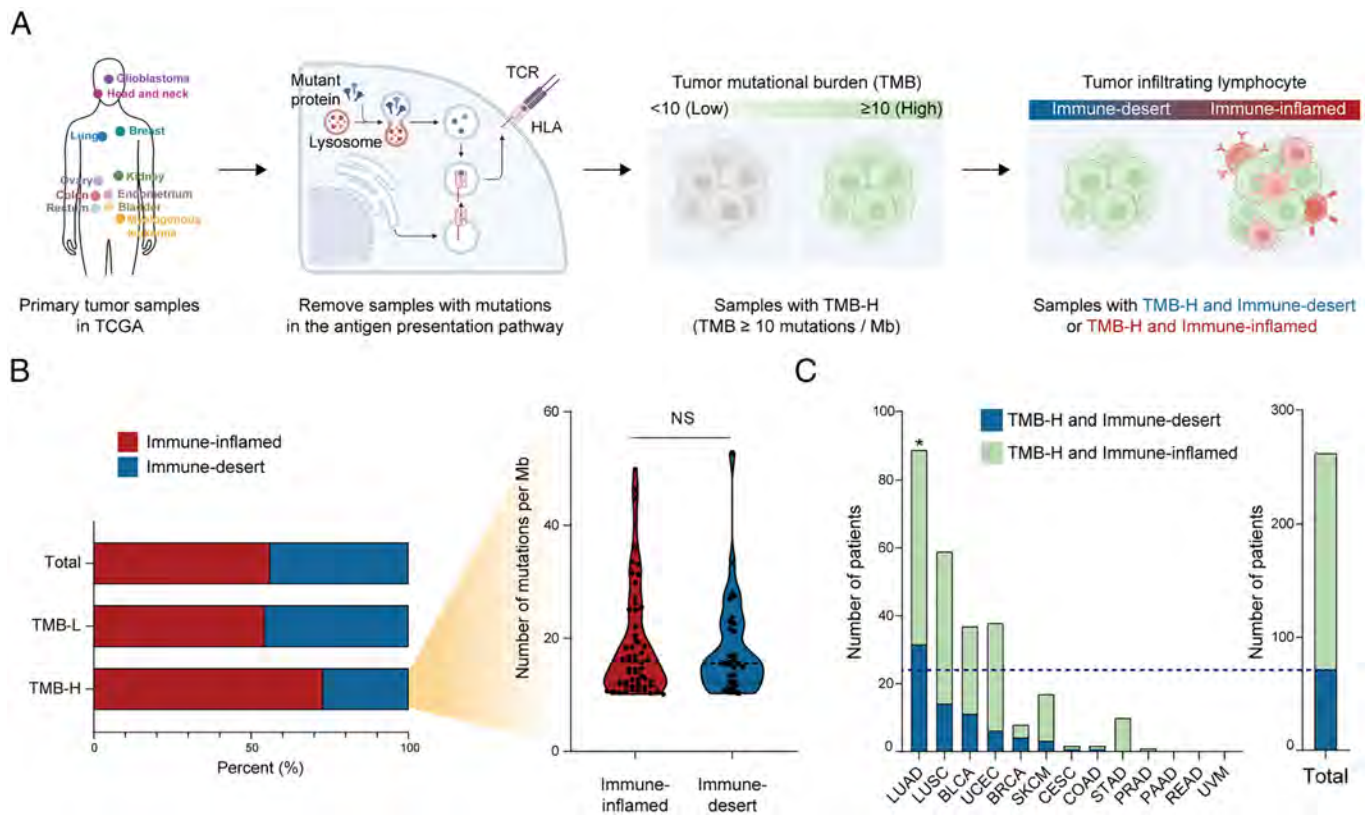
Fig. 1. Despite the highest tumor mutation burden (TMB-H), lung adenocarcinoma (LUAD) has the largest proportion of samples with very low lymphocyte infiltration (i.e., immune-desert) within the tumor mass in The Cancer Genome Atlas (TCGA) data. (*A*) A schematic illustration of identifying the immune-desert or immune-inflamed groups within TMB-H samples from the TCGA is presented. The immune-desert group with TMB-H is characterized as a cluster displaying a high number of mutations and a low population of immune cells, despite the absence of mutations in the antigen presentation pathway. Using the previous classification data based on the degree of tumor-infiltrating lymphocytes from TCGA H&E images (12), we classified the cancer samples into "TMB-H and immune-desert" and "TMB-H and immune-inflamed." (*B*) The bar plot shows the percentage of immune-inflamed and immune-desert phenotypes across all samples in TCGA, further divided into total, low tumor mutation burden (TMB-L), and TMB-H groups (*Left*). The number of mutations per Mb in immune-inflamed and immune-desert phenotype samples within the TMB-H group is not significantly different (*Right*). (*C*) The bar plot illustrates the distribution of patients in immune-inflamed and immune-desert samples with high TMB across various tumor types. Notably, the LUAD group significantly exhibits the highest number of immune-desert samples in contrast to other cancer types (hypergeometric test, *$P < 0.05$).

(*SI Appendix*, Table S1*A*) and immune-inflamed (*SI Appendix*, Table S1*B*) phenotypes of TMB-H lung cancers).

To further investigate the roles of DDX54 as a master regulator, we analyzed the DDX54 regulon and regulons of pivotal TFs regulated by DDX54 (*SI Appendix*, Table S2). The regulatory relationships of multiple TFs and genes regulated by DDX54 were visualized in the GRN (Fig. 2*E*). Using gene ontology (GO) and GSEA, it was found that the genes regulated by DDX54 are associated with several immune evasion pathways, including oncogenic properties activated by the WNT, NF-κB, Myc, and Jak-STAT3 pathways, as well as EMT and embryonic stem cell signatures (Fig. 2*F* and *SI Appendix*, Fig. S4, using public lung cancer RNA-seq data such as GSE81089 and GSE171415). The analysis further identified gestational and trophoblast signatures associated with immune tolerance between mother and fetus (27) (*SI Appendix*, Fig. S5). Moreover, an analysis of clinical data (28) from patients treated with anti-PD1 or anti-PD-L1 therapies reveals that the expression levels of DDX54 significantly stratify patients in terms of overall survival and progression-free survival (*SI Appendix*, Fig. S6). Based on these findings, we postulate that DDX54 could serve as a master regulator responsible for the immune-desert characteristics of lung cancer cells with TMB-H.

Knockdown of DDX54 Suppresses Diverse Oncogenic Pathways by Induction of Tumor Suppressor microRNA Expression. DDX54 is known to be associated with the posttranscriptional regulation in colorectal and breast cancers (29, 30). To assess the transcriptomic

regulation effects of DDX54 loss (*SI Appendix*, Fig. S7*A*), we examined the transcriptome changes according to DDX54 expression levels. It turns out that suppressing DDX54 markedly upregulated genes involved in microRNA biogenesis, notably Drosha and Dicer (Fig. 3*A*). We further compared microRNA profiles between wild-type Ddx54 (WT Ddx54) and Ddx54 knockdown (Ddx54 KD) in LLC1 cells. Ddx54 KD significantly elevated microRNA expressions, such as mmu-miR-34b-5p an established tumor suppressor microRNA (11) (Fig. 3*B*).

To further investigate the roles of the top three microRNAs upregulated by Ddx54 KD, we constructed a comprehensive microRNA-mRNA regulation map, and searched for the presence of conserved sites that match the seed region of each microRNA (31) (Fig. 3*C*). This map highlights the microRNA regulons, whose functions we discerned using GO analysis. Of note, these microRNAs downregulated the genes whose signatures are associated with immunosuppression and tumor malignancy, such as the activation of Wnt and Myc pathways, the initiation of EMT, and the elevation of cancer stemness (Fig. 3*D*). From these, we found that microRNAs regulated by Ddx54 play a significant role in the posttranscriptional modification of genes related to immune cell evasion associated with the Wnt or Myc pathways (32, 33), as well as EMT (34). Activation of the Myc and Wnt pathways, known to induce cancer cell tumorigenicity, concurrently triggers various immune evasion mechanisms in cancer cells. Myc activation hinders immune surveillance, leading to the dysregulation of the tumor microenvironment (TME) and evasion of the host immune response (33). Similarly, the Wnt
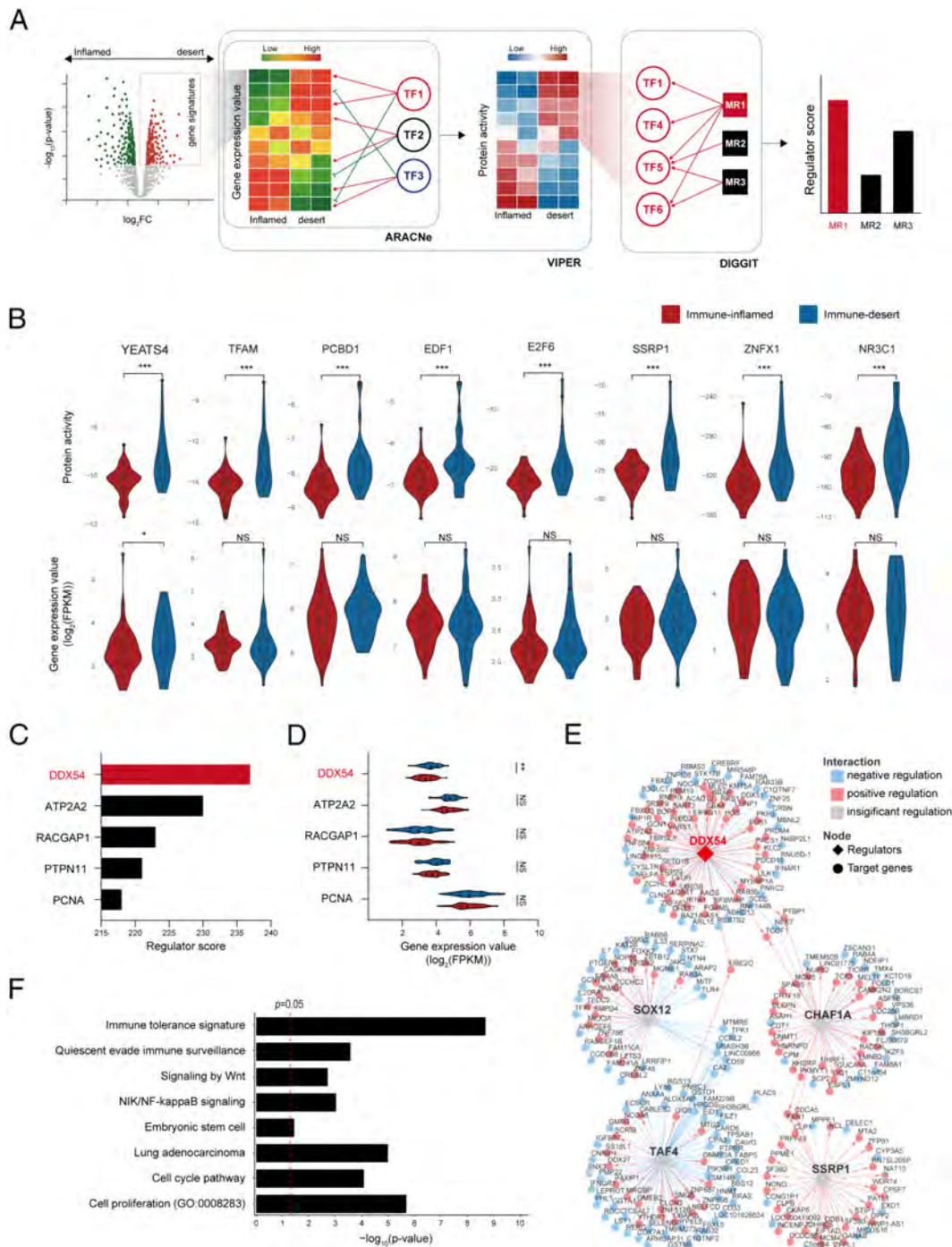
Fig. 2. Identification of DDX54 as the master regulator that governs immune-desert phenotypes of TMB-H lung cancers. (*A*) A schematic procedure illustrating how we identified the master regulator that governs immune-desert phenotypes in TMB-H lung cancer. To identify the master regulator, we applied ARACNe, VIPER, and DIGGIT sequentially (18–20). (*B*) The violin plots show protein activity levels (*Top*) and gene expression levels (*Bottom*) of the top 8 pivotal TFs candidates that significantly regulate gene signatures of the immune-desert phenotype by VIPER analysis (Wilcoxon rank-sum test: *$P < 0.05$, ***$P < 0.001$, and NS: not significant) (both protein activities and gene expression data for all TF candidates are summarized in *SI Appendix*, Fig. S3). (*C*) The bar plot illustrates the scores of candidate master regulators (For further details, refer to the *Detailed Methods* in *SI Appendix*). Of note, DDX54 holds the highest rank among these regulators. (*D*) The violin plot shows gene expression levels of the master regulator candidates across the immune-inflamed and immune-desert groups. DDX54 turns out to be the sole master regulator with a significant expression difference between the two groups (Wilcoxon rank-sum test: **$P < 0.01$ and NS: not significant). (*E*) Visualization of the network derived from the ARACNe algorithm (20), showing DDX54 regulon as well as the regulons of the other top four genes with the highest regulator mode of action scores among the TFs in *SI Appendix*, Fig. S3. (*F*) GO analysis result of target genes regulated by DDX54. The bar plot shows that DDX54 might regulate genes with signatures related to immune evasion, embryonic stem cells, WNT and NF-κB pathways, cell proliferation, and LUAD.

pathway impedes immune cell infiltration (32). Moreover, alterations such as enhanced EMT and increased stemness of cancer cells also contribute to immune evasion. Our investigation identified three microRNAs—nmu-miR-34b-5p, nmu-miR-6240, and nmu-miR-3544-5p—that regulate the expression of various immune evasion-related pathways outlined above. In particular, bolstering these malignancy pathways has been recognized to enhance resistance to anti-PD1 therapy. Moreover, among the three microRNAs, the orthologous microRNA hsa-miR-34b-5p, identified in human lung cancer, is upregulated in immune-inflamed lung cancer tissues with TMB-H. In addition, we found that this microRNA regulates the expression of various immune evasion-related pathways, consistent with its role in LLC1 mice (*SI Appendix*, Figs. S8 *A* and *B*). Together, Ddx54 KD might decrease ICI resistance by promoting the

expression of tumor-suppressive microRNAs (Fig. 3*E*). We note, however, that this potential mechanism was only investigated by in vitro experiments and remains to be further validated in vivo.

Knockdown of DDX54 Synergizes with an Anti-PD1 Treatment in Suppressing Tumor Growth of ICI-Resistant Mouse Lung Cancer Cells. While cancers with TMB-H are frequently recognized as nonself by immune cells, Ddx54 orchestrates several oncogenic pathways, facilitating the evasion of these cells from immune surveillance. This enables cancer cells to elude immune detection and develop resistance to immunotherapy. With this understanding, we aimed to ascertain whether targeting Ddx54 could mitigate resistance to ICI therapy and facilitate tumor regression by enhanced immune cell infiltration. To validate Ddx54 as a potential
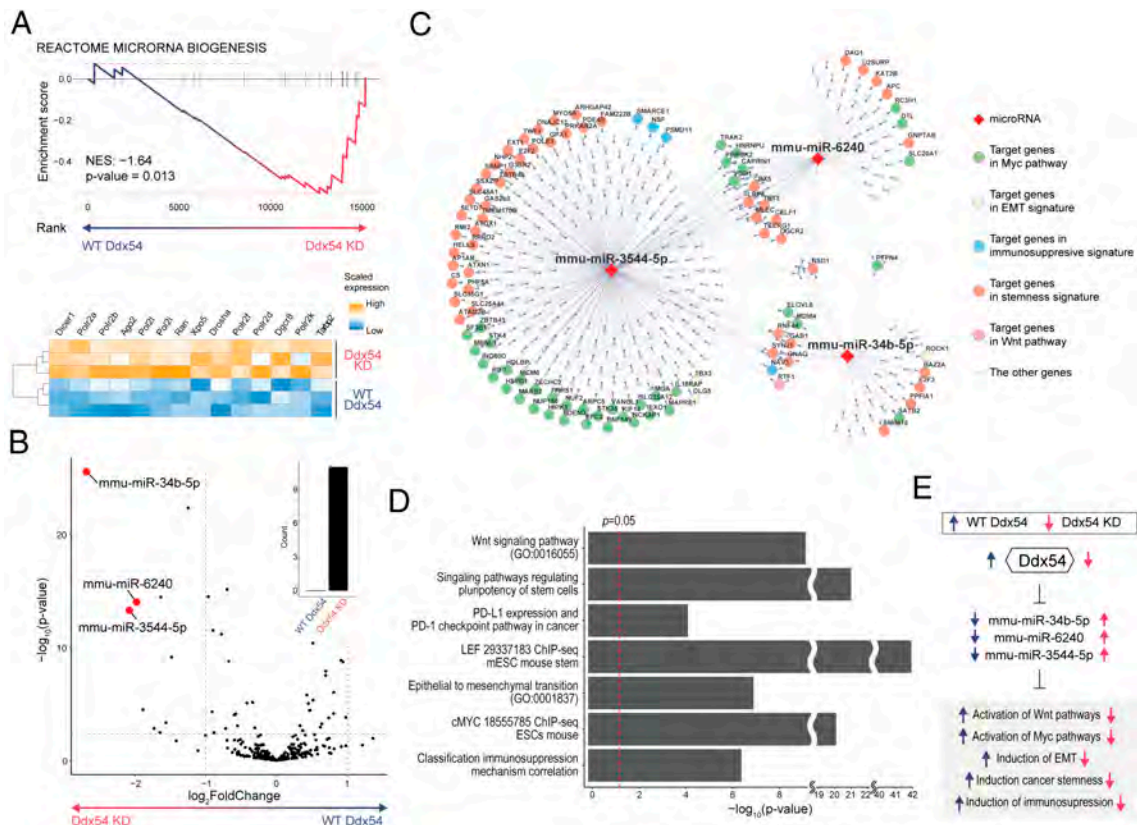
Fig. 3. MicroRNAs regulated by Ddx54 inhibit diverse gene signatures associated with immune evasion. (*A*) The enrichment plot indicates that the knockdown (KD) of Ddx54 leads to the upregulation of genes associated with the microRNA genesis (*Top*). The heatmap visualizes the normalized gene expression of the representative genes related to the microRNA genesis (*Bottom*). (*B*) The volcano plot shows the differentially expressed microRNAs in wild-type (WT) Ddx54 compared to Ddx54 KD. The bar plot shows the number of microRNAs that exhibit significant changes after Ddx54 KD in LLC1 cells (*Top* and *Right* in Fig. 3B). Among these, the three microRNAs significantly up-regulated by Ddx54 KD are denoted by red dots in the plot. Ddx54 KD resulted in a significant increase in the expression levels of nmu-miR-34b-5p, nmu-miR-6240, and nmu-miR-3544-5p. (*C*) A network map showing the interactions between the three microRNAs and their predicted target mRNAs. Red diamonds symbolize microRNAs, and circles denote predicted target mRNAs. The color-coding of circles depicts the pathways constituted by the target genes. (*D*) A bar plot showing that genes predicted to be regulated by the three microRNAs correspond to multiple immune evasion-related gene signatures. (*E*) A schematic diagram illustrating the regulatory relationship among Ddx54, microRNAs, and predicted target gene signatures. Ddx54 activates oncogenic pathways and immune evasion signatures by suppressing the expression of three microRNAs in vitro.

combination target for ICI therapy, we established a syngeneic mouse model using LLC1 lung cancer cells, characterized by both resistance to ICI therapy and TMB-H (Fig. 4*A*). Interestingly, Ddx54 KD cells with anti-PD1 antibody treatment produced much smaller tumors than those from WT Ddx54 cells with anti-PD1 antibody treatment, whereas either anti-PD1 treatment alone or Ddx54 KD alone had no significant effect on tumors from WT Ddx54 cells (Fig. 4*B*). In our experiments, treatment with an anti-PD1 antibody on Ddx54 KD cells significantly promoted the reduction in cancer cell proliferation, evident not only in reduced tumor volume but also in metrics like tumor weight and improved survival rates in the syngeneic mouse model (Fig. 4 *B–D* and *SI Appendix*, Figs. S11 and S12). In addition, to further examine the effect of Ddx54 suppression in mitigating the therapeutic resistance to anti-PD1, we established additional syngeneic mouse models using CRISPR-based knockout of Ddx54 in LLC1 and KLN205 cells and investigated the effects of anti-PD1 antibody treatment (Fig. 4 *G–J* and *SI Appendix*, Figs. S11 *A–D*). In validation experiments, Ddx54 downregulation combined with anti-PD-1 antibody treatment significantly reduced the proliferation of LLC1 and KLN205 cells in syngeneic mouse models (Fig. 4 *B–D* and *SI Appendix*, Fig. S11 and S12), whereas the effect of Ddx54 downregulation was less pronounced in the absence of immune checkpoint blockade in vitro (*SI Appendix*, Fig. S10). Together, these results suggest that combining Ddx54 KD with anti-PD1 antibody treatment can overcome resistance to ICI therapy.

Knockdown of Ddx54 and Simultaneous Anti-PD1 Treatment Effectively Lead to Antitumor Lymphocyte Infiltration In Vivo. The combination of Ddx54 knockdown and anti-PD1 therapy effectively inhibits cancer cell proliferation in the syngeneic mouse model. We found that the reduction cancer cell proliferation is associated with an increase in the infiltration of immune cells, particularly CD8 T cells, through the quantification of tumor-infiltrating lymphocytes in whole slide images (Fig. 4*E* and *SI Appendix*, Fig. S13A) and flow cytometry analysis (Fig. 4*F* and *SI Appendix*, Fig. S13B). To further investigate it, we examined the characteristics of infiltrated immune cells within the tumor tissues in our syngeneic model, by generating spatial transcriptome data of the tumor tissues (Fig. 5*A*) as well as measuring single-cell transcriptome of infiltrated Cd45 immune cells isolated from the tumor tissues (Fig. 5*H* and *SI Appendix*, Fig. S15; For further details, refer to the *Detailed Methods* in *SI Appendix*). First, using spatial transcriptomic data, we investigated the types and amounts of TILs across four conditions. Interestingly, Ddx54 knockdown combined with anti-PD1 treatment can increase the infiltration of antitumor lymphocytes such as T cells, NK cells, B cells, and dendritic cells (DCs) (Fig. 5 *B–G* and *SI Appendix*, Fig. S14), as shown by previous image inference and flow cytometry analysis (Fig. 4 *E* and *F*). In particular, while anti-PD1 treatment alone can recruit lymphocytes, it does not induce their infiltration into the core of tumor tissues. In contrast, Ddx54 knockdown alone effectively induces the infiltration of antitumor lymphocytes
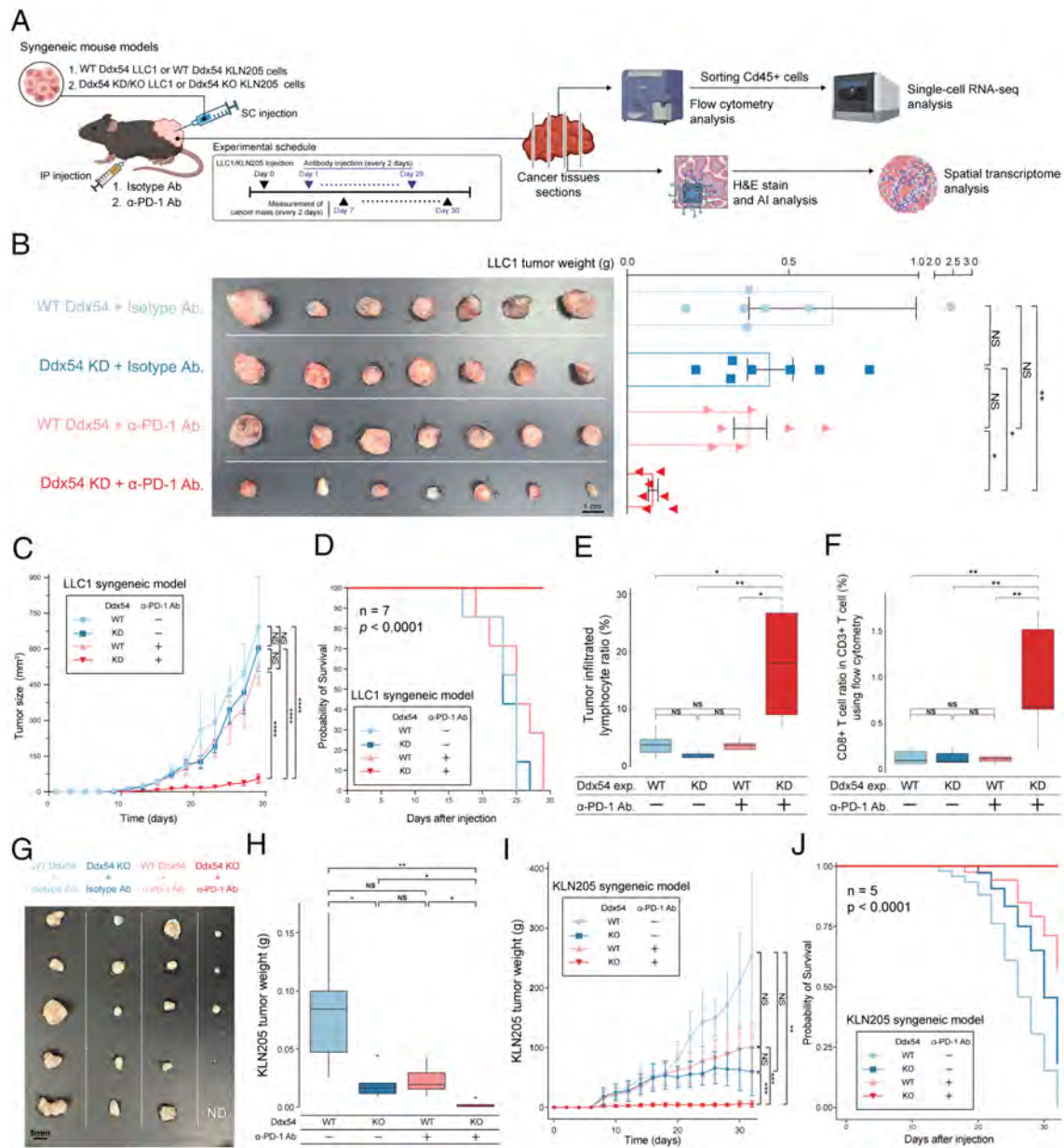
Fig. 4. Knockdown of Ddx54 leads to mitigation of resistance to anti-PD1 treatment in syngeneic mouse models using LLC1 and KLN205 cells. (*A*) Experimental design to assess the effect of Ddx54 knockdown on the resistance to anti-PD1 therapy in syngeneic mouse models using LLC1 and KLN205 cells. (*B–F*) Ddx54 knockdown reduces LLC1 resistance to anti-PD-1 therapy in a syngeneic mouse model, significantly promoting tumor regression by increasing tumor-infiltrating lymphocytes and Cd8 T cells. (*B*) The image showing the resected tumor masses from the syngeneic mice at the endpoint. The bar plot illustrates the distribution of the weights of tumors at the point of extraction. (*C*) The growth curve showing tumor volume changes in the syngeneic mice over time. Time-course analysis of the growth ratios in LLC1 cells after wild-type/knockdown Ddx54 or treatment with isotype/anti-PD1 antibodies. (*D*) The Kaplan–Meier survival plot of LLC1 tumor-bearing mice treated with anti-PD1 treatment. In particular, all of the syngeneic LLC1 mice that received both Ddx54 knockdown and anti-PD1 treatment at the same time showed complete survival. (*E*) Inferred quantification of tumor-infiltrating lymphocytes in whole slide images (35) under the four conditions. Box plot of the quantified ratio of TILs across four conditions. (*F*) Flow cytometry analysis quantifies the ratio of Cd8 T cells in Cd3 lymphocytes under the four conditions. Cd8 T cells infiltrate into lung cancer tissues treated with simultaneous Ddx54 knockdown and anti-PD-1 treatment. (*G–J*) Ddx54 knockout mitigates anti-PD1 therapy resistance in the KLN205 syngeneic mouse model. (*G*) The image depicts the resected tumor masses from the syngeneic mice at the endpoint. (*H*) The bar plot illustrates the distribution of tumor weights at the extraction time. (*I*) The growth curve shows tumor volume changes in syngeneic mice over time, including a time-course analysis of growth ratios in KLN205 cells after wild-type/knockout Ddx54 or treatment with isotype/anti-PD1 antibodies. (*J*) The Kaplan–Meier survival plot represents KLN205 tumor-bearing mice treated with anti-PD1. Notably, all syngeneic KLN205 mice that received both Ddx54 knockout and anti-PD1 treatment exhibited complete survival. Data are presented as the mean ± SEM [independent experiments, n = 7 (LLC1 syngeneic mouse model), n = 5 (KLN205 syngeneic mouse model), ANOVA with the Bonferroni post hoc test: *$P < 0.05$, **$P < 0.01$, ***$P < 0.001$, ****$P < 0.0001$, and NS: not significant; ND: not detected]. *SI Appendix*, Fig. S11 presents the results of repeated experiments using the Ddx54 knockdown LLC1 syngeneic mouse model, and *SI Appendix*, Fig. S12 shows the results obtained from the Ddx54 knockout LLC1 syngeneic mouse model.

into the core of tumor tissues compared to anti-PD1 treatment (Panels 2 and 3 in Fig. 5*B* and *SI Appendix*, Fig. S14). Second, the QC-passed single-cell data were then annotated based on established marker profiles (Fig. 5 *I* and *J* and *SI Appendix*, Fig. S15). As a result, we observed compositional alterations in tumor-infiltrating lymphocytes within Ddx54 knockdown cancer

masses that were concurrently treated with anti-PD1 antibody. In particular, the simultaneous combined knockdown of Ddx54 and anti-PD1 markedly augmented the infiltration of T cells, B cells, and DCs—all pivotal in decreased proliferation of cancer cells (Fig. 5 *K* and *L*). Given that Ddx54 is understood to regulate attributes of cancer cells that are perceived as nonself yet exhibit
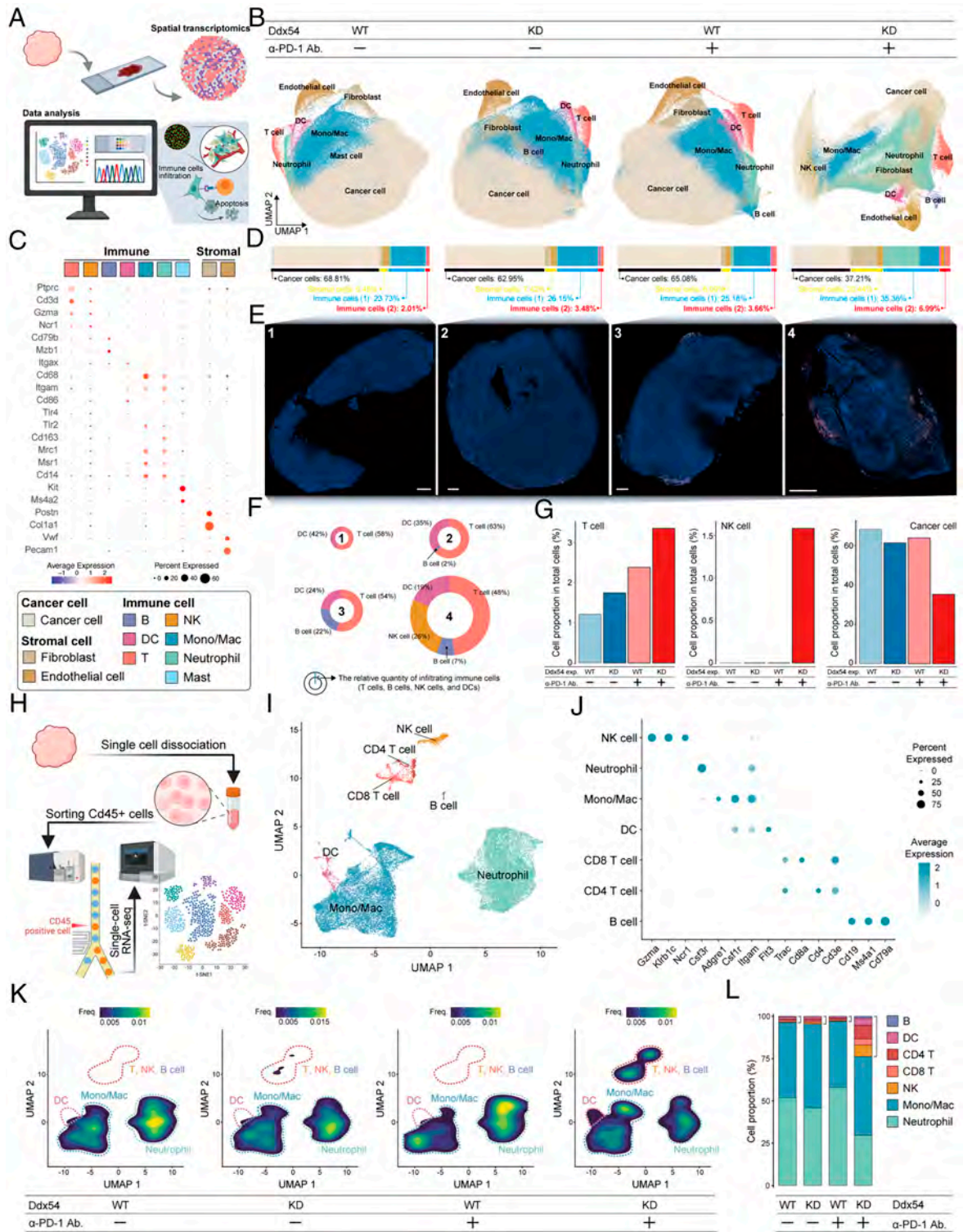
Fig. 5. Simultaneous treatment of Ddx54 knockdown with anti-PD1 treatment promotes T cell infiltration into cancer tissues. (*A*) The schematic figure showing how we obtained the positional and transcriptomic information of each cell constituting the cancer tissue in the syngeneic mouse model. (*B*) Uniform Manifold Approximation and Projection (UMAP) embedding of single cells in the cancer tissues from the syngeneic mouse model annotated by cell types using spatial transcriptome data. (*C*) The dot plot illustrating the scaled average expression of marker genes across distinct cell types. (*D*) Bar plots showing the proportion of each cell type in the cancer tissue from the syngeneic mouse model under four conditions (WT Ddx54 without or with anti-PD1 treatment, and Ddx54 KD without or with anti-PD1 treatment). (*E*) The tissue images showing infiltrated T cells, B cells, NK cells, and DCs in each of the LLC1 cancer tissues across four conditions. While the total number of infiltrated immune cells is similar between the Ddx54 knockdown and anti-PD-1 groups, Ddx54 knockdown facilitates more effective infiltration into tumor tissues. (*F*) The proportion of infiltrated immune cells relative to total cancer cells is represented by the radius of each pie chart. Moreover, the individual immune cell types constituting the immune cell group are indicated separately. (*G*) Bar plots showing the proportion of T cells, NK cells, and cancer cells under four conditions. (*H*) A schematic diagram illustrating how we quantified and characterized the immune cells infiltrated into tumor tissue. Single-cell transcriptome data were produced by isolating Cd45+ immune cells from the tumor mass using a flow cytometry sorter. (*I*) UMAP embedding of single-cell transcriptomes for infiltrated Cd45+ immune cells annotated by cell types. (*J*) The dot plot illustrating the scaled average expression of marker genes across distinct cell types (For further details, refer to the *Detailed Methods* in *SI Appendix*). (*K*) Density plots present UMAP embeddings of Cd45+ cells across four conditions. (*L*) A bar plot showing the proportion of each cell type in Cd45+ immune cells under four conditions. The brackets show the proportion of anticancer immune cells.

limited immune cell infiltration, the observed transformation from an immune-desert tumor to an immune-inflamed tumor following ICI treatment underscores the therapeutic potential of targeting Ddx54. In summary, we demonstrated that combined suppression of Ddx54 and PD1 effectively curtailed the proliferation of immunotherapy-resistant cancer cells, primarily through enhanced infiltration of various anticancer immune cells (Fig. 5 *G* and *L*). In addition to the changes in lymphoid cells, there were also clear changes in the myeloid population (Fig. 5*K*). These are discussed in detail below.

Ddx54 Induces Cd38- and Cd47-Mediated Immunosuppression and Results in the Immune Escape of Tumor Cells. Ddx54 is known to control the transcriptome abundances of various genes by regulating their stabilization (36). We analyzed transcriptome profiles between WT Ddx54 and Ddx54 KD LLC1 cells and found that Ddx54 KD represses the expression of ICI-resistance signatures (37) (Fig. 6*A* and *SI Appendix*, Fig. S8). This implies that Ddx54 KD can mitigate resistance to ICI therapy. We further investigated the impact of Ddx54 KD on transcriptomic alterations. Similar to the microRNA regulon signatures regulated by Ddx54, Ddx54 increased the expression of EMT, Myc, and stemness-associated signatures at both RNA and protein levels (Fig. 6 *B* and *C*). These signatures have a strong association with immune evasion, resulting in resistance to ICI therapy.

Resistance to ICI therapy arises from the advent of an immune-suppressive environment due to the increased expression of immunomodulatory proteins in tumor cells. To probe this mechanism, we assessed the alterations in the expression of immune evasion proteins upon Ddx54 KD (Fig. 6 *E* and *G*). We found that Ddx54 KD leads to a diminished expression of certain immunomodulatory proteins. In particular, Cd38, which regulates adenosine production, FcγR-related resistance, and antibody-dependent cellular cytotoxicity mediated by natural killer (NK) cells (40), and Cd47, which inhibits phagocytosis and interactions with SIRPα of monocytes and macrophage, which can inhibit antigen presentation to T cell, thereby inactivating T cell repones, are significantly decreased (41). Each of these immune modulators is regarded as a potent target for immunotherapy, either as standalone agents or in combination, and they are currently under clinical evaluation for their effects on T cell responses. Consequently, the reduced expression of pivotal immunomodulators such as Cd38 and Cd47, coupled with the reduction of gene signatures associated with resistance to various immunotherapies via Ddx54 knockdown, suggests that Ddx54 could serve as a combination target to enhance the efficacy of ICI therapy.

Signaling Mechanisms of Cd38 and Cd47 Expression Regulated by Ddx54. Ddx54 acts as a master regulator of several oncogenic pathways (Fig. 2), primarily through the modulation of microRNA expression and RNA stability (Fig. 3). Notably, Ddx54 seems to orchestrate an environment conducive for cancer cells to elude immune cell surveillance by governing the expression of Cd38 and Cd47. In this context, we delineated the mechanism through which Ddx54 influences the expression of Cd38 and Cd47, as evident from transcriptomic alterations. The expression of Cd47 is modulated by the activity and expression of Myc, Stat3, and NF-κB (38, 39). These factors can bind to the enhancer region of Cd47, thereby inducing its expression (Fig. 6 *D* and *E*). We then investigated whether Ddx54 can regulate those pathways. Intriguingly, Ddx54 KD attenuated the activity of both the Stat3 and NF-κB pathways and reduced Myc expression signatures at both RNA and protein levels. We also note that NF-κB is a TF governing the expression of Cd38. Therefore, suppression

of NF-κB pathway by Ddx54 KD might explain the observed reduction of Cd38 expression in cancer cells (Fig. 6 *F* and *G*). This downregulation of CD38 and CD47 following the knockdown of DDX54 is observed not only in the LLC1 mouse lung cancer cells but also in the KLN205 mouse lung cancer cells and the A549 human lung cancer cells (*SI Appendix*, Figs. S8*C* and S12 *E* and *F*). Taken together, we concluded that multiple oncogenic pathways regulated by Ddx54 may enable cancer cells to evade immune surveillance through upregulation of EMT and stemness and contribute to resistance against ICI therapy through the modulation of Cd38 and Cd47 expression (Fig. 6*H*).

The Knockdown of Ddx54, in Combination with Anti-PD1 Treatment, Decreases the Population of Protumor Monocytes while Increasing that of Antitumor Monocytes. Monocytes and macrophages play a crucial role in orchestrating anticancer responses within the TME (42). Notably, knockdown of Ddx54 concurrently suppresses the expression levels of Cd38 and Cd47, alongside various oncogenic pathways. This suggests that Ddx54 knockdown may modulate the populations of monocytes and macrophages. To explore this possibility, we further investigated the characteristics of infiltrated monocytes.

By analyzing the single-cell transcriptome of monocytes, we identified six subtypes of monocytes through manual annotation based on marker gene expression (Fig. 7 *A* and *B* and *SI Appendix*, Fig. S16; for further details, refer to the *Detailed Methods* in *SI Appendix*). One of the clusters exhibited increased expression of angiotensin-converting enzyme (ACE) (Fig. 7*B*). Upregulation of ACE is known to promote M1 activation of monocytes, thereby enhancing cellular and humoral immune responses (43). Consequently, this induces an antitumor phenotype in the mouse cancer model. Interestingly, the population of M1-like monocytes, which can engulf and kill cancer cells and present antigens to T cells, increases significantly with the simultaneous knockdown of Ddx54 and anti-PD1 treatment (Fig. 7 *C*, *D*, and *E*). In contrast, the proportion of circulating monocytes, which produce adenosine, secrete Tgf-β, and upregulate immune checkpoints and modulators, decreases upon Ddx54 knockdown alone (Fig. 7 *C*, *D*, *F*, and *G*). Circulating monocytes are particularly associated with resistance to ICI therapy (44). From these findings, we concluded that Ddx54 increases the number of circulating monocytes, which contributes to the construction of an immunosuppressive TME, thereby suppressing the infiltration and differentiation of M1-like monocytes (Fig. 7*H*).

The Conversion of an Immune-Desert Tumor into an Immune-Inflamed Tumor by Ddx54 Knockdown Combined with Anti-PD1 Treatment. The knockdown of Ddx54, combined with anti-PD1 treatment, suppresses various immune evasion mechanisms employed by cancer cells and increases the composition of antitumor monocytes and antitumor T cells. To characterize these infiltrating T cells, in particular, in terms of early effector T markers and exhausted T cells, we annotated T cells in spatial transcriptomic data (Fig. 8 *A* and *B*). Intriguingly, the combination of Ddx54 knockdown and anti-PD1 treatment increases effector and memory Cd4/Cd8 T cells, while decreasing exhausted Cd4/Cd8 T cells and regulatory Cd4 T cells (Fig. 8 *C* and *D*).

In summary, these findings reveal that Ddx54 knockdown, in conjunction with anti-PD1 treatment, orchestrates a shift in the tumor immune microenvironment by simultaneously reducing the population of circulating monocytes and promoting the presence of M1-like monocytes. This transformation is accompanied by an increase in effector and memory CD4/CD8 T cells, which are critical for effective antitumor immunity, and a concomitant
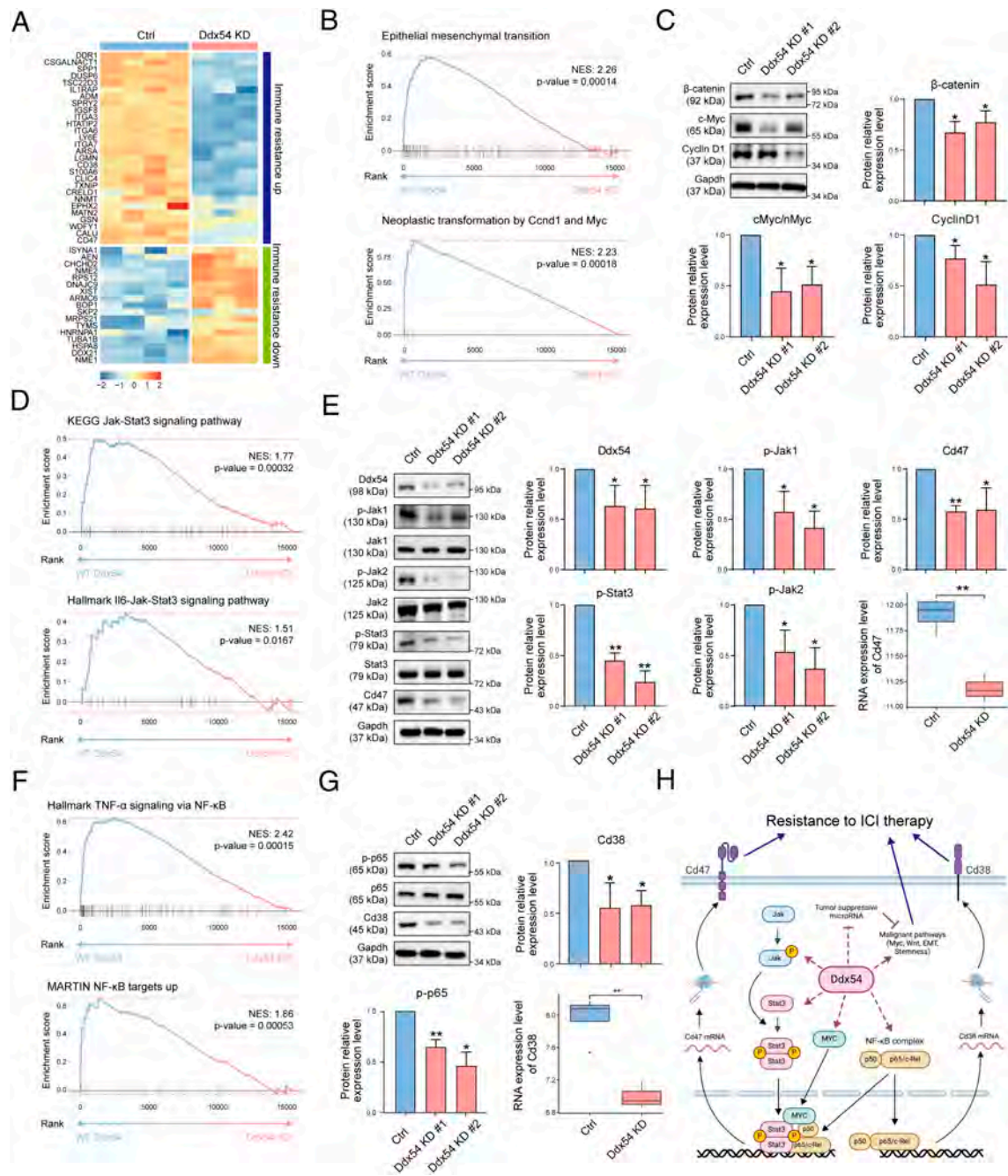
Fig. 6. Molecular mechanisms underlying Ddx54-mediated resistance to immune checkpoint inhibitor (ICI) therapy. (*A*) The heatmap shows normalized expression profiles of immune resistance-associated genes (37) obtained by comparing WT Ddx54 and Ddx54 KD cells (n = 4 for WT Ddx54; n = 3 for Ddx54 KD) (For further details, refer to the *Detailed Methods* in *SI Appendix*). (*B* and *C*) Ddx54 expression leads to activation of the epithelial–mesenchymal transition (EMT) and Myc pathway in LLC1 cells. (*B*) The enrichment plot illustrates the GSEA results of EMT and Myc pathways. (*C*) Protein abundances were monitored by western blotting analysis of the representative genes of EMT and Myc pathways (β-catenin, Myc, Cyclin D1). Gapdh was used as a loading control. (*D* and *E*) Ddx54 induces Cd47 expression through activation of Jak-Stat3. (*D*) GSEA results of Jak-Stat3 associated signatures. (*E*) Protein abundances were monitored by western blotting analysis of the representative genes of Jak-Stat3 pathways (Jak1, Jak2, Stat3, and Cd47). Gapdh was used as a loading control. (*F* and *G*) Ddx54 results in increased expression levels of Cd38 by activation of NF-κB pathway. (*F*) GSEA results of NF-κB associated signatures. (*G*) Protein abundances were monitored by western blotting analysis of the representative genes of NF-κB pathways (p-p65, p65, and Cd38). Gapdh was used as a loading control. (*H*) A schematic diagram illustrating that Ddx54 induces Cd38 and Cd47 expression through activations of Myc, Jak-Stat3, and NF-κB pathways (38, 39). Through these pathways, Ddx54 leads to expression of immune escape signatures. Data are presented as the mean ± SEM (n = 3 independent experiments, two-tailed *t* test: *$P < 0.05$, **$P < 0.01$, and ***$P < 0.001$).

reduction in exhausted CD4/CD8 T cells and regulatory CD4 T cells, both of which are associated with immune suppression. As a result, the knockdown of Ddx54, combined with anti-PD1, ultimately leads to the conversion of an immune-desert tumor into an immune-inflamed tumor and thereby mitigates resistance to ICIs (Fig. 8*E*). Together, these changes highlight the therapeutic potential of targeting Ddx54 to enhance antitumor immunity and overcome immune evasion mechanisms.

Discussion

Tumor mutational burden (TMB) is the latest FDA-approved pan-cancer biomarker for anti-PD1 therapy (8). Multiple meta-analyses showed TMB as a reliable predictive biomarker (9, 48), but the response rate for melanoma patients on ICI therapy, whose tumors exhibit TMB-H (≥10 mutations/Mb), is only 41% (49). Such a limited response is caused by the fact that some cancer tissues with
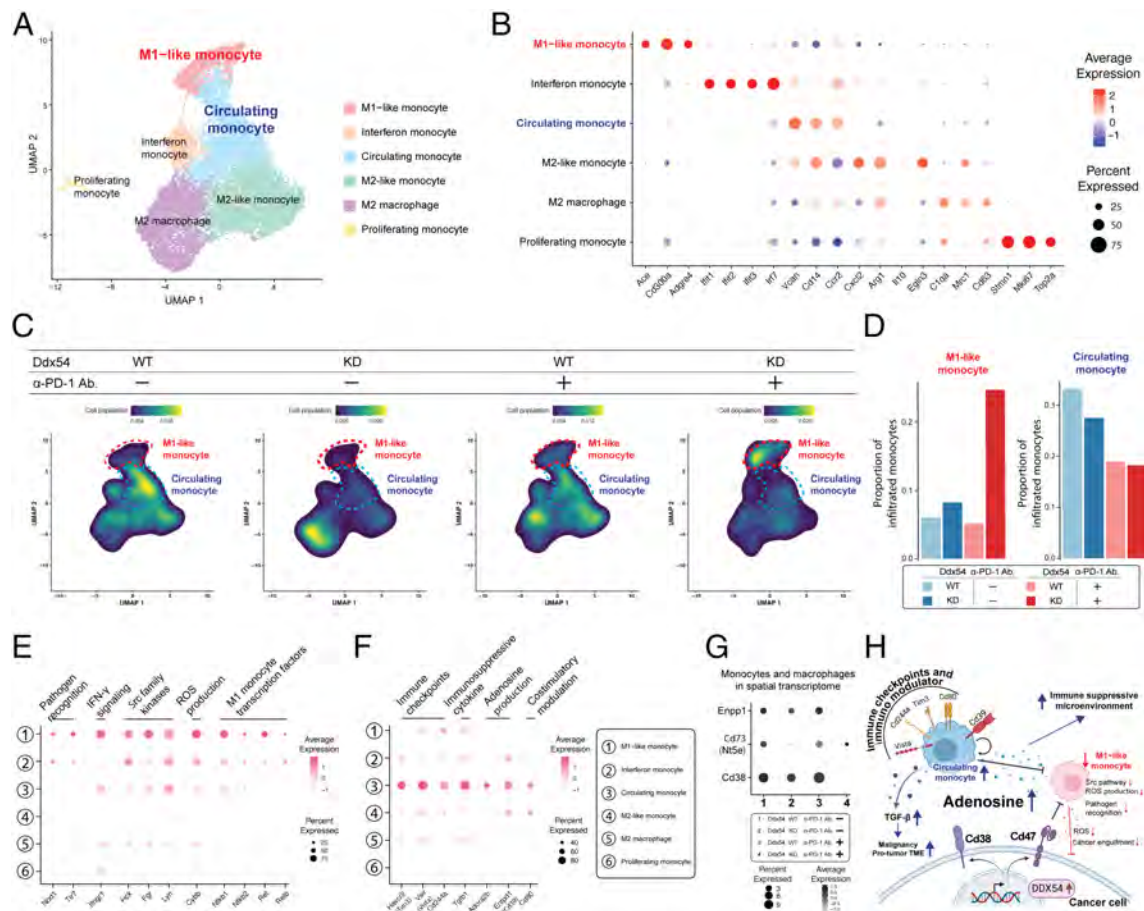
Fig. 7. Ddx54 expression enhances the infiltration of circulating monocytes while suppressing the infiltration of M1-like monocytes. (*A*) UMAP embedding of single-cell transcriptomes shows monocytes and macrophages categorized by cell subtypes. (*B*) The dot plot presenting the scaled average expression levels of marker genes across the different cell subtypes (For further details, refer to the *Detailed Methods* in *SI Appendix*). (*C*) Density plots illustrate UMAP embeddings of monocytes and macrophages across four conditions and (*D*) bar plots indicate the proportions of each cell subtype within monocytes and macrophages under the four conditions. The M1-like monocyte population is particularly increased in the Ddx54 KD and anti-PD1 treatment group, while the circulating monocyte population decreases in the Ddx54 KD groups. (*E*) The genes associated with M1-like monocytes in immune-supportive tumor microenvironment (TME) exhibit increased expression, also including the genes involved in pathogen recognition, reactive oxygen species (ROS) production, and transcription factors specific to M1 monocytes. (*F*) Circulating monocytes in immune-suppressive TME show increased expression of the genes associated with immune checkpoints, immunosuppressive cytokines, adenosine pathways, and costimulatory modulation. (*G*) In the spatial transcriptome analysis, Ddx54 knockdown combined with anti-PD1 treatment shows reduced expression of the genes linked to adenosine production. (*H*) Ddx54 knockdown decreases the infiltration of circulating monocytes while increasing the infiltration of M1-like monocytes. Circulating monocytes exhibit elevated expression of Tgf-β (45), genes associated with adenosine production, immune checkpoints (46) (Vista, Cd244a, and Tim3), and Cd80 (47), all of which can suppress immune functions.

TMB-H can still effectively suppress immune infiltration. This is a critical issue for immunotherapy since immune inflammation is directly associated with increased response to ICI therapy (50). This study attempts to convert immune-desert tumors with TMB-H into immune-inflamed ones by controlling the master regulator that governs the immune evasive strategies of TMB-H cancers.

The immune-desert cancer with TMB-H acquires various oncogenic phenotypes simultaneously to escape from immune cells. From a therapeutic perspective, blocking all these pathways individually is infeasible. Thus, we aimed to identify the master regulator that can collectively govern and regulate these immune evasive pathways. For this purpose, we constructed and analyzed lung cancer gene regulatory networks at the system level to identify potential master regulators. As a result, DDX54 was identified as the master regulator with the highest regulator score. Interestingly, other regulator candidates that we also found such as ATP2A2, RACGAP1, PTPN11, and PCNA were previously reported (23–26) to regulate immunotherapy responses or to be associated with evading immune surveillance.

We found that DDX54 induces expression of CD38 and CD47 by activation of MYC, JAK-STAT, and NF-κB pathways. These clusters of differentiation proteins are known to block the infiltration of immune cells (40, 41). In particular, CD38 acts as an

ectoenzyme that breaks down extracellular nicotinamide adenine dinucleotide (NAD⁺) into metabolites like ADP-ribose (ADPR) and cyclic ADP-ribose (cADPR), inducing an immunosuppressive TME (51). By depleting NAD⁺, CD38 inhibits proliferation, cytokine production, and cytotoxic activity of T cells (52). In addition, the increased levels of ADPR and cADPR disrupt calcium signaling in immune cells, leading to reduced activation and diminished effector functions (52). Furthermore, we revealed that DDX54 represses the expression of several tumor-suppressive microRNAs, which in turn reduce immune-evasive signatures in cancer cells. However, further investigations are needed to clarify how DDX54 directly regulates microRNA expression. Based on these, we demonstrated that DDX54 knockdown mitigates resistance to ICI therapy in a syngeneic mouse model.

During tumorigenesis, cancer hijacks various mechanisms used in early embryogenesis that must be repressed after development (53). Many maternal and placental immunomodulatory factors are required for adequate placental invasion, such as the trophoblast that surrounds the embryoblast to evade maternal immunological attack. Similar transcriptomic features are observed in the LLC1 model we used. However, DDX54 knockdown induces a significant reduction in these features of the early fetal trophoblast
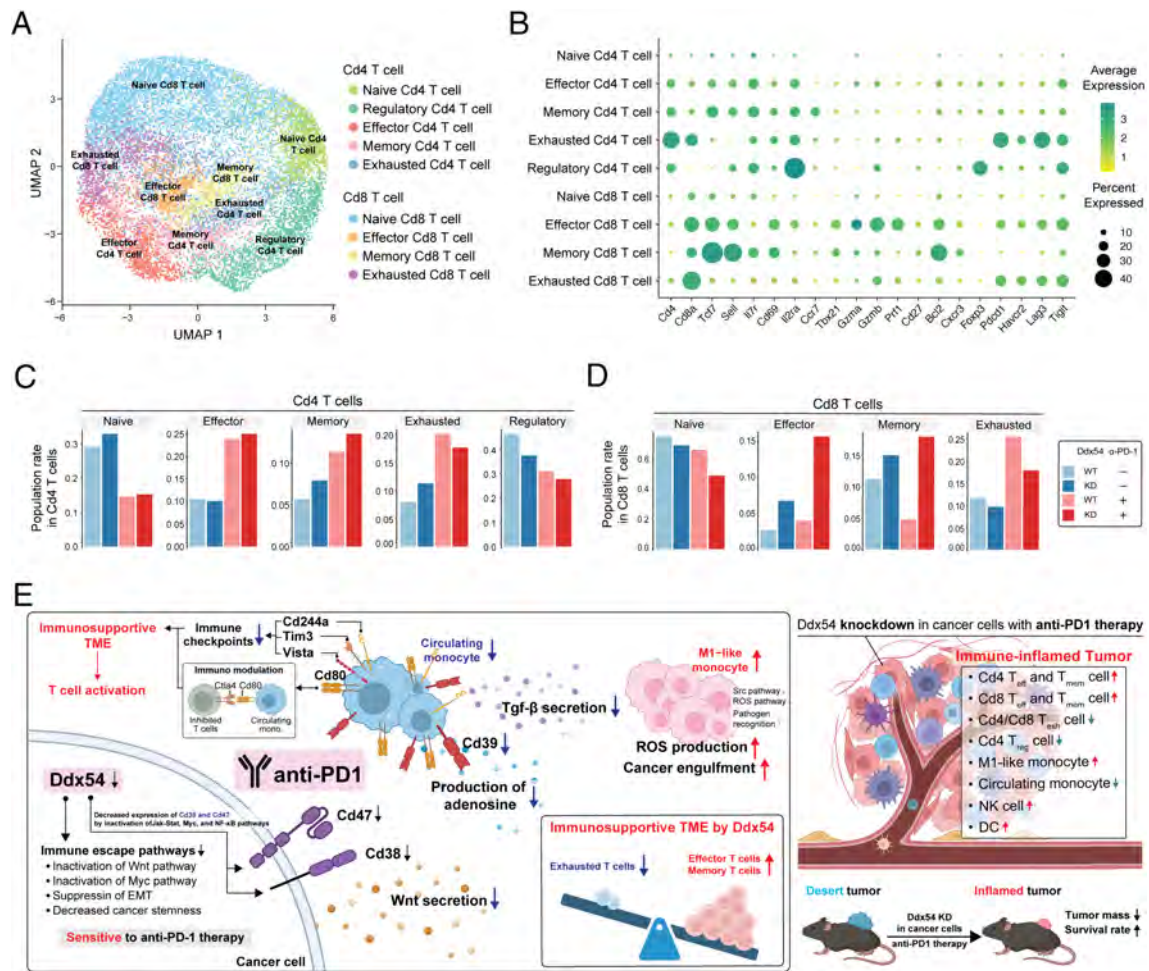
Fig. 8. Ddx54 knockdown combined with anti-PD1 treatment promotes effector and memory T cell differentiation while reducing exhausted and regulatory T cell populations. (*A*) UMAP embedding of spatial transcriptome data illustrates Cd4 and Cd8 T cell subtypes, including naïve, effector, memory, and regulatory T cells. (*B*) The dot plot presenting the expression levels of marker genes specific to Cd4 and Cd8 T cell subtypes. (*C*) Effector and memory Cd4 T cells are increased, whereas exhausted and regulatory Cd4 T cells are reduced in the Ddx54 KD and anti-PD1 treatment group. (*D*) Effector and memory Cd8 T cells are increased, whereas exhausted Cd8 T cells are reduced in the Ddx54 KD and anti-PD1 treatment group. (*E*) The schematic figure depicts the remodeling of lymphoid and myeloid compartments under Ddx54 knockdown and anti-PD1 treatment, illustrating the conversion of an immune-suppressive TME into an immune-supportive one, thereby enhancing the therapeutic effects of anti-PD1 treatment. Abbreviations: Effector T cell (T_{eff} cell), Memory T cell (T_{mem} cell), Exhaustion T cell (T_{exh} cell), Regulatory T cell (T_{reg} cell), Natural killer cell (NK cell), and dendritic cell (DC).

(*SI Appendix*, Fig. S5). This leads us to speculate that cancer hijacks the immune evasion mechanism in early fetal development by turning on DDX54 in LLC1 cells, such that its knockdown allows the infiltration of immune cells.

A number of strategies have been suggested to stimulate immune responses against cancer, ranging from ICIs to T or NK cellular therapies (4). In addition, cancer vaccines have been developed to improve the recognition of specific cancer antigens by the immune system (54). However, all these immunotherapies are only effective for a limited number of cancer patients. Moreover, their efficacy is significantly reduced in solid tumors compared to hematological malignancies. To overcome such an obstacle, immune cells should be able to infiltrate into solid tumor tissues to trigger apoptosis of malignant cells. This study found that the immune-suppressive master regulator, DDX54, can change the immune-desert TME into the immune-inflamed one. Indeed, DDX54 knockdown promoted significant immune cell infiltration into the immunotherapy-resistant LLC1 cell line, resulting in effective immunotherapy in vivo. Therefore, we expect to overcome the current limitation of existing immunotherapy by identifying and regulating immune evasion master regulators, such as DDX54.

We showed that Ddx54 knockdown combined with anti-PD1 treatment effectively mitigates resistance to ICI therapy using the syngeneic mouse model. However, there still remain some limitations of this study for clinical applicability. First, since significant differences exist between human and mouse immune systems (55), the findings from syngeneic mouse models have limitations in their direct translation to clinical applications. Future studies may need further validation using humanized mice with human immune systems (56) or human lung cancer organoid models containing resident human immune cells (57). Second, another limitation of this study is the use of subcutaneous, nonorthotopic lung tumors since the location of the tumor can influence vascularity and leukocyte infiltration, potentially affecting therapeutic responses. Third, to translate the result of this study into gene therapy, we may need advanced delivery technology. Recombinant adeno-associated virus (rAAV)-based vectors and lipid nanoparticle (LNP) systems hold promising potential for selectively targeting lung cancer cells expressing DDX54. So, future studies are needed to fully establish their feasibility for patients. Last, future studies will be needed to determine the percentage of tumor cells that would need to have Ddx54 knockdown or deletion for translational application.

The approach we devised in this study to detect DDX54 by comparing the samples exhibiting high versus low levels of immune cell infiltration can serve as a general framework for identifying potential immune-suppressive master regulators. In particular,

overall T cell infiltration was used in this study as a measure to predict the effectiveness of immunotherapy. We note, however, that the presence of memory T cells, memory-like NK cells, or tertiary lymphoid structures have also been suggested as more advanced biomarkers for immunotherapeutic outcomes (4). In summary, by elucidating and controlling the mechanisms by which cancer cells evade surveillance of immune cells based on these various markers, we may be able to identify another immuno-oncotarget. As such, the proposed approach has numerous applications across immuno-oncology that go beyond the use of infiltration of T cells shown here as examples to improve immunotherapy.

Materials and Methods

Detailed methods are provided in the *SI Appendix*.

Author affiliations: ᵃDepartment of Bio and Brain Engineering, Korea Advanced Institute of Science and Technology, Daejeon 34141, Republic of Korea

Author contributions: K.-H.C. designed research; J.-R.G., J.L., and K.-H.C. performed research; J.-R.G. contributed new reagents/analytic tools; J.-R.G., J.L., Y.H., and K.-H.C. analyzed data; and J.-R.G., J.L., and K.-H.C. wrote the paper.

1. K. J. Hiam-Galvez, B. M. Allen, M. H. Spitzer, Systemic immunity in cancer. *Nat. Rev. Cancer* **21**, 345–359 (2021).
2. F. S. Hodi *et al.*, Improved survival with ipilimumab in patients with metastatic melanoma. *N. Engl. J. Med.* **363**, 711–723 (2010).
3. R. Ferrara *et al.*, Hyperprogressive disease in patients with advanced non-small cell lung cancer treated with PD-1/PD-L1 inhibitors or with single-agent chemotherapy. *JAMA Oncol.* **4**, 1543–1552 (2018).
4. A. D. Waldman, J. M. Fritz, M. J. Lenardo, A guide to cancer immunotherapy: From T cell basic science to clinical practice. *Nat. Rev. Immunol.* **20**, 651–668 (2020).
5. K. M. Mahoney, P. D. Rennert, G. J. Freeman, Combination cancer immunotherapy and new immunomodulatory targets. *Nat. Rev. Drug Discov.* **14**, 561–584 (2015).
6. K. B. Yates *et al.*, Epigenetic scars of CD8(+) T cell exhaustion persist after cure of chronic infection in humans. *Nat. Immunol.* **22**, 1020–1029 (2021).
7. K. E. Yost *et al.*, Clonal replacement of tumor-specific T cells following PD-1 blockade. *Nat. Med.* **25**, 1251–1259 (2019).
8. A. Marabelle *et al.*, Association of tumour mutational burden with outcomes in patients with advanced solid tumours treated with pembrolizumab: Prospective biomarker analysis of the multicohort, open-label, phase 2 KEYNOTE-158 study. *Lancet Oncol.* **21**, 1353–1365 (2020).
9. D. Sha *et al.*, Tumor mutational burden as a predictive biomarker in solid tumors. *Cancer Discov.* **10**, 1808–1825 (2020).
10. S. Spranger, T. F. Gajewski, Impact of oncogenic pathways on evasion of antitumour immune responses. *Nat. Rev. Cancer* **18**, 139–147 (2018).
11. X. Bai, L. Zheng, Y. Xu, Y. Liang, D. Li, Role of microRNA-34b-5p in cancer and injury: How does it work? *Cancer Cell Int.* **22**, 381 (2022).
12. J. Saltz *et al.*, Spatial organization and molecular correlation of tumor-infiltrating lymphocytes using deep learning on pathology images. *Cell Rep.* **23**, 181–193 e187 (2018).
13. J. H. Shim *et al.*, HLA-corrected tumor mutation burden and homologous recombination deficiency for the prediction of response to PD-(L)1 blockade in advanced non-small-cell lung cancer patients. *Ann. Oncol.* **31**, 902–911 (2020).
14. D. J. McGrail *et al.*, High tumor mutation burden fails to predict immune checkpoint blockade response across all cancer types. *Ann. Oncol.* **32**, 661–672 (2021).
15. M. Muquith *et al.*, Tissue-specific thresholds of mutation burden associated with anti-PD-1/L1 therapy benefit and prognosis in microsatellite-stable cancers. *Nat. Cancer* **5**, 1121–1129 (2024), 10.1038/s43018-024-00752-x.
16. E. O. Paull *et al.*, A modular master regulator landscape controls cancer transcriptional identity. *Cell* **184**, 334–351.e320 (2021).
17. P. Cahan *et al.*, Cell net: Network biology applied to stem cell engineering. *Cell* **158**, 903–915 (2014).
18. M. J. Alvarez, J. C. Chen, A. Califano, DIGGIT: A Bioconductor package to infer genetic variants driving cellular phenotypes. *Bioinformatics* **31**, 4032–4034 (2015).
19. M. J. Alvarez *et al.*, Functional characterization of somatic mutations in cancer using network-based inference of protein activity. *Nat. Genet.* **48**, 838–847 (2016).
20. A. A. Margolin *et al.*, ARACNE: An algorithm for the reconstruction of gene regulatory networks in a mammalian cellular context. *BMC Bioinformatics* **1**, S7 (2006).
21. Y. Deng *et al.*, Glucocorticoid receptor regulates PD-L1 and MHC-I in pancreatic cancer cells to promote immune evasion and immunotherapy resistance. *Nat. Commun.* **12**, 7041 (2021).
22. X. Sun *et al.*, Overexpression of CHAF1A is associated with poor prognosis, tumor immunosuppressive microenvironment and treatment resistance. *Front Genet* **14**, 1108004 (2023).
23. Y. Cao, H. Duan, A. Su, L. Xu, B. Lai, A pan-cancer analysis confirms PTPN11's potential as a prognostic and immunological biomarker. *Aging (Albany NY)* **14**, 5590–5610 (2022).
24. R. A. Eid *et al.*, Assessment of RACGAP1 as a prognostic and immunological biomarker in multiple human tumors: A multiomics analysis. *Int. J. Mol. Sci.* **23**, 14102 (2022).
25. C. Y. Hong *et al.*, Sarcoplasmic reticulum Ca(2+) ATPase 2 (SERCA2) reduces the migratory capacity of CCL21-treated monocyte-derived dendritic cells. *Exp. Mol. Med.* **48**, e253 (2016).
26. K. Kundu *et al.*, Inhibition of the NKp44-PCNA immune checkpoint using a mAb to PCNA. *Cancer Immunol. Res.* **7**, 1120–1134 (2019).
27. S. G. Holtan, D. J. Creedon, P. Haluska, S. N. Markovic, Cancer and pregnancy: Parallels in growth, invasion, and immune modulation and implications for cancer therapeutic agents. *Mayo Clin. Proc.* **84**, 985–1000 (2009).
28. J. Kang *et al.*, Systematic dissection of tumor-normal single-cell ecosystems across a thousand tumors of 30 cancer types. *Nat. Commun.* **15**, 4067 (2024).
29. B. C. McKay, Post-transcriptional regulation of DNA damage-responsive gene expression. *Antioxid Redox Signal* **20**, 640–654 (2014).
30. M. Milek *et al.*, DDX54 regulates transcriptome dynamics during DNA damage response. *Genome Res.* **27**, 1344–1359 (2017).
31. S. E. McGeary *et al.*, The biochemical basis of microRNA targeting efficacy. *Science* **366**, eaav1741 (2019).
32. S. Spranger, R. Bao, T. F. Gajewski, Melanoma-intrinsic beta-catenin signalling prevents anti-tumour immunity. *Nature* **523**, 231–235 (2015).
33. R. Dhanasekaran *et al.*, The MYC oncogene—the grand orchestrator of cancer growth and immune evasion. *Nat. Rev. Clin. Oncol.* **19**, 23–36 (2022).
34. A. Dongre *et al.*, Epithelial-to-mesenchymal transition contributes to immunosuppression in breast carcinomas. *Cancer Res.* **77**, 3982–3989 (2017).
35. S. Abousamra *et al.*, Deep learning-based mapping of tumor infiltrating lymphocytes in whole slide images of 23 types of cancer. *Front. Oncol.* **11**, 806603 (2021).
36. Y. Yu *et al.*, DDX54 plays a cancerous role through activating P65 and AKT signaling pathway in colorectal cancer. *Front. Oncol.* **11**, 650360 (2021).
37. L. Jerby-Arnon *et al.*, A cancer cell program promotes T cell exclusion and resistance to checkpoint blockade. *Cell* **175**, 984–997.e924 (2018).
38. S. C. Casey, V. Baylot, D. W. Felsher, The MYC oncogene is a global regulator of the immune response. *Blood* **131**, 2007–2015 (2018).
39. C. Y. Huang, Z. H. Ye, M. Y. Huang, J. J. Lu, Regulation of CD47 expression in cancer cells. *Transl. Oncol.* **13**, 100862 (2020).
40. Y. Li, R. Yang, L. Chen, S. Wu, CD38 as an immunomodulator in cancer. *Future Oncol.* **16**, 2853–2861 (2020).
41. M. E. W. Logtenberg, F. A. Scheeren, T. N. Schumacher, The CD47-SIRPalpha Immune Checkpoint. *Immunity* **52**, 742–752 (2020).
42. A. Mantovani, P. Allavena, F. Marchesi, C. Garlanda, Macrophages as tools and targets in cancer therapy. *Nat. Rev. Drug Discov* **21**, 799–820 (2022).
43. Z. Khan *et al.*, Overexpression of the C-domain of angiotensin-converting enzyme reduces melanoma growth by stimulating M1 macrophage polarization. *J. Biol. Chem.* **294**, 4368–4380 (2019).
44. B. P. Keenan *et al.*, Circulating monocytes associated with anti-PD-1 resistance in human biliary cancer induce T cell paralysis. *Cell Rep.* **40**, 111384 (2022).
45. D. V. F. Tauriello, E. Sancho, E. Batlle, Overcoming TGFbeta-mediated immune evasion in cancer. *Nat. Rev. Cancer* **22**, 25–44 (2022).
46. X. He, C. Xu, Immune checkpoint signaling and cancer immunotherapy. *Cell Res.* **30**, 660–669 (2020).
47. M. J. Butte, M. E. Keir, T. B. Phamduy, A. H. Sharpe, G. J. Freeman, Programmed death-1 ligand 1 interacts specifically with the B7-1 costimulatory molecule to inhibit T cell responses. *Immunity* **27**, 111–122 (2007).
48. M. D. Hellmann *et al.*, Tumor mutational burden and efficacy of nivolumab monotherapy and in combination with ipilimumab in small-cell lung cancer. *Cancer Cell* **33**, 853–861.e854 (2018).
49. C. Valero *et al.*, Response rates to anti-PD-1 immunotherapy in microsatellite-stable solid tumors with 10 or more mutations per megabase. *JAMA Oncol.* **7**, 739–743 (2021).
50. J. Galon, D. Bruni, Approaches to treat immune hot, altered and cold tumours with combination immunotherapies. *Nat. Rev. Drug Discov.* **18**, 197–218 (2019).
51. Q. Liu, I. A. Kriksunov, R. Graeff, H. C. Lee, Q. Hao, Structural basis for formation and hydrolysis of the calcium messenger cyclic ADP-ribose by human CD38. *J. Biol. Chem.* **282**, 5853–5861 (2007).
52. V. Bocuzzi *et al.*, CD38 as theranostic target in oncology. *J. Transl. Med.* **22**, 998 (2024).
53. T. M. Malta *et al.*, Machine learning identifies stemness features associated with oncogenic dedifferentiation. *Cell* **173**, 338–354.e315 (2018).
54. M. J. Lin *et al.*, Cancer vaccines: The next immunotherapy frontier. *Nat. Cancer* **3**, 911–926 (2022).
55. Z. B. Bjornson-Hooper *et al.*, A comprehensive atlas of immunological differences between humans, mice, and non-human primates. *Front. Immunol.* **13**, 867015 (2022).
56. J. Chuprin *et al.*, Humanized mouse models for immuno-oncology research. *Nat. Rev. Clin. Oncol.* **20**, 192–206 (2023).
57. R. Polak, E. T. Zhang, C. J. Kuo, Cancer organoids 2.0: Modelling the complexity of the tumour immune microenvironment. *Nat. Rev. Cancer* **24**, 523–539 (2024).
58. J. Gong, J. Lee, K. Cho, DDX54 inhibition enhances anti-PD1 therapy in immune-desert lung tumors with high tumor mutational burden. Gene Expression Omnibus. http://www.ncbi.nlm.nih.gov/geo/query/acc.cgi?acc=GSE268555. Deposited 29 May 2024.
59. J. Gong, J. Lee, K. Cho, DDX54 inhibition enhances anti-PD1 therapy in immune-desert lung tumors with high tumor mutational burden. Gene Expression Omnibus. http://www.ncbi.nlm.nih.gov/geo/query/acc.cgi?acc=GSE285341. Deposited 26 December 2024.
60. J. Gong, J. Lee, K. Cho, DDX54 inhibition enhances anti-PD1 therapy in immune-desert lung tumors with high tumor mutational burden. Gene Expression Omnibus. http://www.ncbi.nlm.nih.gov/geo/query/acc.cgi?acc=GSE285342. Deposited 26 December 2024.
61. J. Gong, J. Lee, K. Cho, DDX54 inhibition enhances anti-PD1 therapy in immune-desert lung tumors with high tumor mutational burden. Gene Expression Omnibus. http://www.ncbi.nlm.nih.gov/geo/query/acc.cgi?acc=GSE289119. Deposited 9 February 2024.